

# On-Device CPU Scheduling for Sense-React Systems

Aditi Partap  
aditi712@stanford.edu  
Stanford University

Samuel Grayson  
grayson5@illinois.edu  
University  
of Illinois at Urbana-Champaign

Muhammad Huzaiifa  
huzaiifa2@illinois.edu  
University  
of Illinois at Urbana-Champaign

Sarita Adve  
sadve@illinois.edu  
University  
of Illinois at Urbana-Champaign

Brighten Godfrey  
pbg@illinois.edu  
University  
of Illinois at Urbana-Champaign

Saurabh Gupta  
saurabhg@illinois.edu  
University  
of Illinois at Urbana-Champaign

Kris Hauser  
kkhauser@illinois.edu  
University  
of Illinois at Urbana-Champaign

Radhika Mittal  
radhikam@illinois.edu  
University  
of Illinois at Urbana-Champaign

## Abstract

Sense-react systems (e.g. robotics and AR/VR) have to take highly responsive real-time actions, driven by complex decisions involving a pipeline of sensing, perception, planning, and reaction tasks. These tasks must be scheduled on resource-constrained devices such that the performance goals and the requirements of the application are met. This is a difficult scheduling problem that requires handling multiple scheduling dimensions, and variations in resource usage and availability. In practice, system designers manually tune parameters for their specific hardware and application, which results in poor generalization and increases the development burden. In this work, we highlight the emerging need for scheduling CPU resources at runtime in sense-react systems. We study three canonical applications (face tracking, robot navigation, and VR) to first understand the key scheduling requirements for such systems. Armed with this understanding, we develop a scheduling framework, Catan, that dynamically schedules compute resources across different components of an app so as to meet the specified application requirements. Through experiments with a prototype implemented on a widely-used robotics framework (ROS) and an open-source AR/VR platform, we show the impact of system scheduling on meeting the performance goals for the three applications, how Catan is able to achieve better application performance than hand-tuned configurations, and how it dynamically adapts to runtime variations.

## 1 Introduction

Sense-react systems are becoming ever more pervasive. A variety of robots now assist us with various mundane, high precision, or dangerous tasks [6, 10, 11, 35, 39, 45, 49, 70, 81]. AR/VR (Augmented/Virtual Reality) has affected the way we teach, practice medicine [48, 71], and play games, and is envisioned to be the next interface for compute [66, 76]. These systems typically feature a pipeline of tasks that involve continually sensing the environment and processing the sensed

inputs to generate a reaction. Such a pipeline ranges from a single linear chain of components in the simplest applications to a multi-chain directed acyclic graph (DAG) in more complex ones. Most such systems run on devices with limited compute resources, (e.g. Intel NUC [19, 38], Raspberry Pi [41, 44], Qualcomm Snapdragon XR2 [1], etc.). This work focuses on managing the compute (CPU) resources on such platforms.

Sense-react systems allow the environmental inputs to be sampled and processed at a configurable rate (i.e. the input rate in sense-react systems can be actively controlled, as opposed to being driven by external factors). CPU scheduling for a given sense-react application (app) thus involves tackling two inter-related aspects — how should the available compute resources be divided across different app components, and the rate at which each component should be executed (which includes the input sampling rate).

The appropriate scheduling decision depends on the amount of available CPU resources, the compute usage of each component, and the app’s performance requirements. The scheduler must take into account dynamic variations in compute usage (due to input-dependent computation times) and compute availability (e.g. due to battery constraints). The performance requirements differ along different components of a sense-react app, and involve semantic trade-offs, where the tasks performed by some app components are more critical than others (e.g. in a navigating robot, components responsible for avoiding local collisions are more important than those responsible for global path planning).

As we show in §7, under-utilizing or overloading the system (e.g. by triggering a component too slowly or too fast), and mis-allocating resources (e.g. giving a greater share of resources to a less critical component) impact the app’s performance (that includes the ability of a robot to track a moving object or avoid collisions, or achieving the desired motion-to-photon latency in an AR/VR system).

Despite rich literature in system scheduling, past work falls short of addressing all of the specific challenges of sense-react systems (e.g. the ability and need to configure input rates, handle heterogeneous tasks with differing requirements, and tackle variability in compute usage at different time-scales). Thus compute resource management in such systems remains a challenge in which app developers are provided little help. While there are frameworks and systems that assist in app development (e.g. ROS [30], ILLIXR [13, 66], etc), they leave scheduling decisions entirely up to the developers. Developers, therefore, manually fine-tune their systems to come up with static configurations which generalize poorly across scenarios (and over time) and increase the burden of app development.

To ease the burden of app development and deployment, we build a scheduling framework, Catan, which takes an app’s semantic requirements as initial inputs from the developer, and dynamically schedules the app components at runtime as per the (varying) compute usage and availability. It is easier for the developer to specify the semantic inputs (that are based on domain expertise, and remain unchanged over time and across compute platforms), as opposed to directly configuring the scheduling knobs (that must be adapted based on compute usage and availability).

We begin by studying three different applications (§3) – face tracking, robot navigation and exploration, and virtual reality. Through our case studies, we identify the key design considerations for a sense-react system scheduler (§4), and use the resulting insights to design Catan (§5). Catan adopts a hierarchical approach, making its scheduling decision in two stages – first determining the spatial allocation of CPU cores across app components, and then determining the temporal allocation of CPU slices and the rate of executing different app components. We develop analytical models and heuristics to translate the scheduling decisions into light-weight constraint-optimization problems, that Catan solves periodically at runtime to account for variability in compute usage and availability. Catan can be plugged into existing frameworks for robotics and AR/VR (e.g. ROS and ILLIXR respectively), and can be provided as an optional service to the apps using the framework (§6).

Through our evaluation on the three aforementioned case-studies (§7), we show (i) how scheduling decisions impact application performance, and how Catan can (ii) effectively navigate the semantic trade-offs in performance goals as per the available compute resources, (iii) achieve better performance than the default (hand-tuned) configurations, and (iv) handle variability in compute usage at different timescales.

## 2 Background

**Overview.** We can represent a sense-react application as a directed acyclic graph (DAG), where each node (or vertex) represents a computation task and each edge represents the flow of data between tasks. The source nodes in the DAG (with no incoming edges) are comprised of various sensors, such as a camera, LiDAR, inertial measurement unit (IMU), etc.,

that continually capture environmental inputs. The sink nodes (with no outgoing edges) produce reactions, e.g. actuators in robotics and display in AR/VR. The in-between nodes are responsible for processing the input streams, e.g. by running detection and planning algorithms to determine appropriate reactions to changes in the environment. In most cases, every time a node runs, it uses the latest outputs generated by its predecessor nodes as its inputs (although some apps may have nodes that buffer multiple inputs and batch process them every time they run). DAGs for different applications vary in their complexity. We describe three examples in §3.

**Deployment Platforms.** In many low cost robots, sensors and actuators are attached to a single on-board computer that runs all components in the DAG, often using CPU as the only compute resource [19, 40, 41]. GPUs and other accelerators can be attached at the cost of higher expense and battery usage. In larger robot systems, the nodes may be split across multiple on-board machines [8, 38], or some nodes may be offloaded to edge or cloud servers [29, 65, 69, 90].

While VR headsets have historically offloaded the computation to an attached server [12], the desired solution is to run AR/VR applications on stand-alone devices (e.g. Oculus Go [22] and Quest [23]) equipped with an embedded system [1, 21, 27]. The embedded platforms provide on-board compute: CPUs, GPUs and accelerators such as DSPs.

In this work, we focus on systems using a single on-board computer, with CPU as the only *contended* resource.<sup>1</sup> This covers a broad range of real-world sense-react systems. Extending our work to systems with multiple contended resources (CPU, GPU, memory, and network) is an interesting future direction.

**Development Frameworks.** It is common to use a software *framework* (e.g. [5, 15, 20, 24, 25, 30, 62, 66]) for developing robotics and AR/VR applications. Robot Operating System (ROS) [30, 79] is by far the most popular development framework for robotics, with more than 300K estimated users [36]. It is widely used for developing research prototypes, with industry usage also growing rapidly [3, 4, 7, 16, 70]. It allows developers to program each component of an application individually, and provides communication APIs among those components. ILLIXR (Illinois Extended Reality testbed) is a complete end-to-end open source VR system and research testbed, which provides configurable VR system configurations with widely used system components and workflows [13, 66]. ILLIXR provides an OpenXR [24] interface to the apps, which abstracts over the XR device, runtime, and OS.

The above (open) frameworks leave resource management decisions entirely up to the app developers. Developers manually configure the rate at which different nodes are triggered. CPU scheduling across nodes is left up to the default OS policies, unless explicitly configured by the developer.<sup>2</sup>

<sup>1</sup>Our VR case-study makes use of GPUs for frame display, but, unlike the CPU cores, we assume GPU resources are not contended.

<sup>2</sup>We do not know what scheduling knobs and policies are used in closed-source / proprietary systems, which are heavily engineered nonetheless.

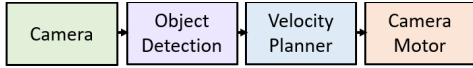


**Figure 1.** DAG representing the face tracking robot app. The colors green, purple, blue and orange represent sensor nodes, perception nodes, planning nodes and actuators respectively

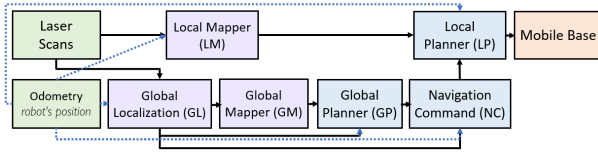


**Figure 2.** DAG representing the robot navigation application.

**Related Dataflow Systems.** DAG abstraction is common across other systems, including real-time [53, 60, 83, 84, 93, 98, 99], sensor nodes [74, 88], and distributed stream processing and dataflow systems [28, 46, 47, 52, 67, 72, 73, 77, 85, 91, 91, 95, 96]. Sense-react systems are distinct from these.

As we show in §4, the computation (execution times) in sense-react systems exhibits a high degree of variability over time — an aspect that conventional real-time systems (based on fixed periodicity) do not handle. In comparison with traditional sensor nodes, sense-react systems have higher processing complexity and variability, which emphasizes the importance of proper CPU scheduling.

Distributed stream-processing systems focus on cluster-wide resource management to handle an incoming stream of queries. We instead focus on CPU scheduling within a single computer on board a robot or a VR device, that runs a single long-running application. Such a system differs in its scheduling knobs and requirements (detailed in §4). For instance, in sense-react systems, the scheduler has greater control over the app, and can actively control the input load.

To summarize, sense-react systems are more dynamic than traditional real-time systems, more complex than sensor nodes, and more controlled than distributed dataflow systems. They thus open an interesting design space for system scheduling.

### 3 Our Case Studies

We use the three representative applications, spanning robotics and AR/VR, as our case studies to inform and evaluate our scheduler design. We briefly describe these applications below.

#### 3.1 Face Tracking Robot

As our first case study, we consider a face-tracking robot implemented using ROS [32, 63]. It involves a rotating camera tasked with tracking a moving object (face). Figure 1 represents the app DAG, which is a simple linear pipeline of the following nodes: (i) a camera to capture and preprocess images, (ii) an object detection node to detect the face in the image, (iii) a planning node to compute the velocity at which the camera must rotate to track the face, and (iv) the camera rotation motor.

**Performance Goals.** The goal of this robot is to always keep the object in its view, i.e. to not lose track of the object.

#### 3.2 Robot 2D Navigation

For our second case study, we consider a robot navigation app implemented using ROS [33], where the robot is tasked with exploring and mapping an unknown area. This is a basic feature that most autonomous mobile robots need to support [86, 97]. This is a more complex app, that involves semantic trade-offs, and higher variations in compute usage over time.

Figure 2 represents the application’s DAG. It uses two sensors — a laser scanner (to capture the environment seen by the robot) and an odometer (which reports speed and location information to all other nodes). The global localization, mapping and planning nodes (GL, GM, and GP) are responsible for planning the robot’s trajectory based on its accumulated knowledge about the area. The trajectory is planned so as to move towards unknown areas for exploration. The local mapping and planning nodes (LM and LP) are responsible for ensuring that the robot avoids collision with obstacles in its immediate vicinity when following the global trajectory. We list the specific function of each processing node below. More details about relevant algorithms can be found in [82, 86].

- (i). The local mapper (LM) uses the laser scans and odometry to update its knowledge about the robot’s immediate vicinity.
- (ii). The global localization node (GL) performs two tasks: (a) for every scan that it receives, it uses particle filtering (Chapter 8 in [86]) to produce an estimated correction for the robot’s location (which accounts for potential drifts in odometry readings), and (b) it then filters the scans, discarding the ones that carry little new information about the environment. Unlike other nodes in the app that always use the latest inputs available from their predecessor nodes, GL buffers the received scans, and batch processes them every time it runs to ensure that all relevant information about the environment is captured.
- (iii) The global mapper (GM) maintains a global map of all the areas that the robot has explored so far. It uses occupancy grid mapping (Chapter 9 in [86]) to update the map based on newly filtered scans produced by GL.
- (iv) The global planner (GP) computes the global trajectory of the robot based on GM’s global map and the robot’s position (derived from the latest correction from GL and the corresponding odometry reading) using graph search (Chapter 3 in [82]).
- (v) Navigation Command (NC) uses the robot’s position, along with the current trajectory (i.e. GP’s output) to decide the direction in which the robot should move.
- (vi) The local planner (LP) uses the local cost map (that contains information about nearby obstacles) and the odometry information, along with the navigation command from NC, to output the robot’s velocity to the actuator (the mobile base).

**Performance Goals.** The foremost goal is to avoid colliding with obstacles. The secondary goal is to ensure that trajectories are planned using the most up-to-date information about the robot’s location and the map, otherwise planned trajectories will be infeasible, unsafe, and inefficient. Finally, the robot should be able to explore the area at a sufficiently high rate.

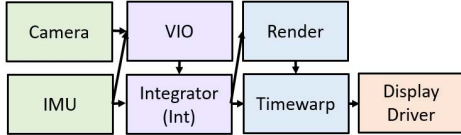


**Figure 3.** DAG representing the VR application in ILLIXR [13, 66]

### 3.3 Virtual Reality

Our final case study considers a different category of sense-react systems – virtual reality (VR) implemented in ILLIXR [13, 66]. The VR system’s task is to provide a smooth visualization of the virtual world, based on the user’s head movement in the real world.

Figure 3 represents the various nodes in a VR system. It uses two sensors: (a) an IMU (inertial measurement unit), which measures acceleration and angular velocity of the user’s head, and (b) a Camera. The Visual-Inertial Odometry node (VIO) uses a localization (SLAM) algorithm to fuse information from the camera and IMU, and produce an estimate of the user’s pose (location and orientation). It generates high accuracy poses but is computationally too expensive to run at a high frequency. To remedy this, the integrator (Int) integrates new samples from the IMU to estimate the change in the pose since the last pose from the VIO. This produces higher frequency, but less accurate, estimates of the user’s pose.

The Render node uses this pose to generate an image (aka a ‘frame’) of the virtual world from the current perspective of the user. However, the latency of the rendering process adds a lag between the user’s movement and the generation and display of the corresponding frame, called the motion-to-photon latency (MTP) [92, 94]. To minimize this latency, the Timewarp node takes the latest rendered frame from Render and the latest pose estimate from Int, and reprojects the frame to be from the latest perspective of the user (reprojecting is much faster than rendering a new frame). Timewarp submits these reprojected frames to the GPU driver which displays them on a head-mounted display at the refresh frequency, based on the display hardware.

The reprojection in the ILLIXR version we use accounts for the user’s rotational motion, but not translational motion. Therefore, we report two MTP metrics - rotational MTP and translational MTP, representing the delay in capturing the user’s rotational and translational motion respectively.<sup>3</sup>

**Performance Goals.** To provide a smooth virtual experience, the primary goal of the scheduler is to ensure that the displayed frame closely tracks the user’s motion with low delay and the best available pose.

Our experiment setup for each of the above case studies uses the apps as implemented in their respective frameworks (ROS for §3.1 and §3.2, and ILLIXR for §3.3). In order to do controlled (repeatable) experiments, we use standard physics

<sup>3</sup>It is difficult to capture the latency of the actual display; we therefore do not include that in our MTP, similar to [66]. With current display technologies, this latency is roughly constant and affects all scheduling mechanisms studied here similarly.

simulators [9, 37] to simulate the sensing and actuation for the two robotics apps (as is standard practice in robotics [54]) – the rest of the processing nodes are executed as in a real system. For VR, ILLIXR supports using offline generated datasets as well as real-time camera and IMU data. For repeatability, we choose to use widely used sensor datasets [56]<sup>4</sup>; the rest of the (real) ILLIXR system is agnostic to this choice. We detail the experiment setup for each case study in §7.

## 4 Design Considerations for CPU Scheduler

We use the above case studies to inform our scheduler design. In this section we list some of the key design considerations.

**Terminology.** First, we will clarify terminology. As mentioned in §2, we use the term *node* to refer to each vertex of the application DAG. We use the term *chain* to denote a unique path from a source node (e.g., a sensor) to a sink node (e.g., the actuator or display) along the DAG. A node may belong to multiple chains. For example, the face-tracking app (Figure 1) comprises of a single chain from the Camera to the Motor. On the other hand, the navigation app (Figure 2) consists of multiple chains from scan and odometry to the mobile base, that pass through different sets of intermediate nodes (e.g. {scans → LM → LP → base}, {scans → GL → NC → LP → base}, {scans → GL → GP → NC → LP → base}, etc). Likewise, the VR DAG (Figure 3) consists of six different chains from Camera and IMU to Display, passing through different intermediate nodes.

### 4.1 Scheduling dimensions

In order to optimize app performance, the CPU scheduler must co-optimize the following key dimensions.

- (i) *Spatial Core Allocation.* Given a multi-core platform, the scheduler must determine how the CPU cores are divided across different components in a sense-react app.
- (ii) *Temporal CPU Allocation.* For a core to which multiple components are assigned, the scheduler must decide how many CPU slices must be allocated to each of them, and how often.
- (iii) *Execution Rate.* For each component, the scheduler must decide the rate at which it is triggered (or executed). This follows from determining the CPU allocation for that component.

We use the term ‘component’ to loosely refer to the granularity at which the scheduler makes its decisions – we discuss this more precisely in §4.2.

### 4.2 Scheduling granularity

We use the term *subchain* to refer to a series of DAG nodes within a chain that run at the same rate in an event-driven manner (with the output from one node triggering the next). Two nodes in a chain would belong to different subchains if there is value to running them at different rates (e.g. if they belong to a different set of chains). Note that each node may be in many chains, but can only belong to one subchain.

<sup>4</sup>We use the sensor dataset to emulate the possible trajectory of a person wearing the VR device. We used the aerial dataset since there is no available dataset for human head movement.

For example, in the navigation DAG (Figure 2), it makes semantic sense for LP to output a new velocity only upon every new input from LM that carries updated knowledge of the robot’s immediate vicinity (and can typically arrive at a faster rate than global navigation commands from NC). Therefore, LP and LM can belong to the same subchain. On the other hand, it is useful to run GP at a higher rate than GM (which is computationally more expensive), allowing the global trajectory to be updated based on updated position estimates.

Since all nodes within a subchain must run at the same rate, a subchain forms the natural granularity at which we can make the scheduling decisions listed in §4.1. The scheduler needs to actively trigger only the first node in each subchain, and each of the remaining nodes in the subchain can be event-triggered when the preceding node produces a new output.<sup>5</sup>

### 4.3 Performance metrics

The scheduling decisions (§4.1) impact the performance goals listed in §3. However, it is difficult for the scheduler to directly reason about app-level performance metrics (e.g. ability to avoid collisions or track a moving object). We instead express different app performance metrics using generalized DAG-level metrics that the scheduler can directly reason about and optimize. Our first metric corresponds to how quickly and frequently new inputs are processed along a given *chain* in the DAG, while the second corresponds to the processing rate of a given *node*. We describe these metrics below:

**Chain Response Time.** It is the worst-case time from the moment a change occurs in the environment, to the moment a reaction is produced at the sink of the chain. We define response time for consecutive pairs of inputs ( $i_{k-1}$  and  $i_k$ ) that are fully processed by the chain to produce new outputs at the sink ( $o_{k-1}$  and  $o_k$  respectively).<sup>6</sup> In the worst case, an environmental change occurs immediately after the source of the chain captures a previous input  $i_{k-1}$  — the system will not react to the change until the next input  $i_k$  is captured and processed by the chain to produce the output  $o_k$ . Chain response time is, therefore, the time difference between when the sink produces a new output  $o_k$ , and when the source captures the *previous* input  $i_{k-1}$ . Intuitively, minimizing response time ( $o_k - i_{k-1}$ ) implies simultaneously minimizing the latency of processing an input along a chain ( $o_{k-1} - i_{k-1}$ ) and maximizing the chain throughput, i.e. minimizing the period ( $o_k - o_{k-1}$ ) between two consecutive outputs.

The robot’s ability to track the moving object for the face tracking app is correlated with the chain’s response time (§7). Likewise, a navigating robot’s ability to avoid collisions is correlated with the response time along the chain ‘scans  $\rightarrow$  LM  $\rightarrow$

<sup>5</sup>This has lower latency than asynchronous triggering of consecutive nodes.

<sup>6</sup>Note that there may be other inputs captured by the chain source between  $i_{k-1}$  and  $i_k$  that get dropped (or overwritten by newer inputs) along the chain and do not influence the output at the sink. Likewise, there may be other outputs between  $o_{k-1}$  and  $o_k$  that use newer inputs along other chains incident at the sink, but are based on input  $i_{k-1}$  from the given chain’s source.

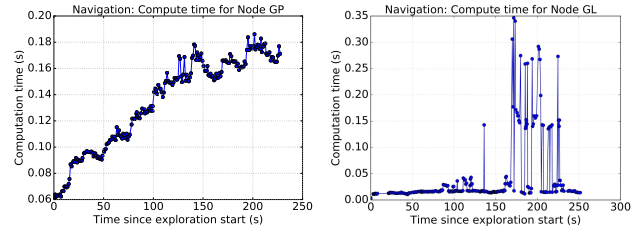


**Figure 4.** Variation in the CPU usage over time of two components in the navigation application: GP (left) and GL (right).

LP  $\rightarrow$  base’, which captures how quickly the robot can react to dynamic obstacles in its immediate vicinity. Minimizing rotational MTP in VR directly translates to minimizing response time along the ‘IMU  $\rightarrow$  Int  $\rightarrow$  Timewarp  $\rightarrow$  Display’ chain. **Node Throughput.** It is the rate at which a given node processes its inputs to produce new outputs. Ensuring that the latest position estimate is available for generating the robot’s trajectory requires high throughput for the GL node (that feeds into multiple other nodes) in the navigation app.

### 4.4 Semantic preferences and constraints

**Preferences across different metrics.** Certain performance metrics are semantically more important than others. For example, in order to avoid collisions during robot navigation, minimizing response times along the local chains must be given highest priority. Next in line is ensuring high GL throughput (to avoid faulty navigation commands derived from stale position information), followed by a sufficiently high throughput for the remaining nodes to minimize the exploration time. Similarly, as detailed in §7, the VR system also involves semantic preferences across the response times for different chains.

**Constraints on different metrics.** An app may require an upper bound on a chain’s response time or a lower bound on a node’s throughput, based on semantic requirements. In addition, a node’s throughput can be upper bounded by the hardware limits of the sensors and actuators/display.

### 4.5 Variations in Compute Usage and Availability

**Variation in compute usage over time.** We use node computation time to capture the amount of CPU consumed by a node every time it runs. We observe that the computation time of some nodes may increase over time. For example, as the navigating robot covers more area, the size of the global map increases, which increases the time taken by (i) GM to update and generate the global map, and (ii) GP to plan the robot’s trajectory based on the map (as shown in Figure 4 (left)).

**Input-dependent variability.** We observe that the GL node for robot navigation has a bimodal computation time — for each laser scan, it either does a quick check and discards it if there is no new information, or processes the scan to update the pose correction. For the frames that were fully processed by GL, we additionally observe occasional spikes in computation times (as shown in Figure 4 (right)). A closer analysis revealed that these spikes arise from a semantic optimization called

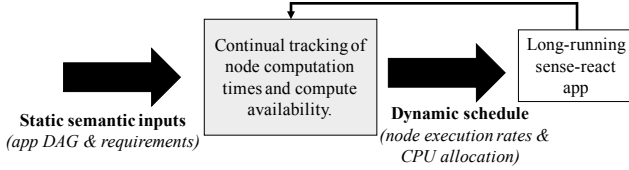


**Figure 5.** High-level workflow of Catan

“loop closure” [14, 86], where on re-visiting a location, the robot runs an expensive non-linear optimization to jointly update the map and all robot poses.

The VIO node in the VR app also shows high variability in compute usage, depending both on the complexity (feature density) of the user’s surroundings and the user’s motion.

**Variation in available compute resources.** The amount of resources available to the application would vary across different hardware platforms. Even for a given platform, the amount of available compute resources may change over the duration of the application run — e.g. as a robot’s battery starts draining over time, the number or frequency of CPU cores can be reduced to save power.

The scheduler must update scheduling decisions over time to account for such variability. Moreover, it must be robust to situations where a node is unable to finish processing an input during its allocated CPU time slices.

#### 4.6 Putting it all together

We design Catan, a CPU scheduler for sense-react application, based on the above considerations. For a given app (represented as a DAG), Catan makes CPU scheduling decisions (§4.1) at the granularity of subchains (§4.2), so as to satisfy the semantic preferences and constraints (§4.4) on chain response times and node throughputs (§4.3), while handling potential variations in compute usage and availability (§4.5).

Figure 5 represents the high-level workflow of Catan. It provides an interface for the app developers to express their semantic requirements. In particular, the developers specify (i) the DAG structure (nodes and edges), (ii) grouping of nodes into subchains, (iii) which metrics must be optimized (i.e. response times of which chains and throughput of which nodes) and the corresponding constraints and weights across these metrics (to capture semantic trade-offs).<sup>7</sup> Catan periodically tracks the per-node computation times and compute availability, and adaptively determines the schedule (node execution rates and CPU allocation), so as to best meet the specified semantic requirements. We detail Catan’s design in §5.

Catan inputs from app developers require significant domain expertise (in the form of thorough understanding of the app requirements). Current frameworks, on the other hand, require app developers to directly configure the low-level scheduling knobs (node execution rates and system scheduling policies) — this requires system-level expertise in addition

<sup>7</sup>Catan allows the developers to optionally specify a few other semantic inputs that we discuss in §5.

to domain expertise. More importantly, the inputs required by Catan are largely independent of the compute availability and usage — they rely only on app semantics and can remain unchanged across deployment platforms and over time. The precise schedule and system-level knobs, on the other hand, must be dynamically adapted based on varying compute usage and availability (§7 shows how static configurations lead to sub-optimal performance). Catan, thus, simplifies the inputs required from app developers by providing a layer of abstraction that translates *static* semantic requirements into a *dynamic* low-level system configuration and schedule.

One could simplify the inputs required from app developers even further by adding hooks to the development framework to infer the DAG structure, inferring subchain grouping based on specified performance constraints and weights, and inferring DAG-level performance requirements from app-level performance requirements. These extensions are beyond the scope of this work, and we leave them for future research.

## 5 Catan Design

We model our scheduling problem as a constrained optimization problem, wherein the objective is a weighted linear combination of the DAG-level metrics (i.e. chain response times and reciprocal of node throughputs). Catan schedules the app subchains, so as to optimize the specified objective and meet any specified constraints.<sup>8</sup>

Catan adopts a hierarchical approach by breaking the scheduling decisions into two stages — the first stage determines the mapping between subchains and cores (§5.1), and the second stage makes scheduling decisions at per-core and per-subchain granularity (§5.2). We begin with outlining our approach under the assumption that the computation time at each node and the number of cores stays constant, and discuss how we handle variability in §5.3.

### 5.1 Stage I: Core Allocation

For a DAG with  $N$  subchains on a system with  $K$  cores, Catan’s first stage of optimization outputs a boolean matrix of size  $N \times K$ , where an element  $a_{ij}$  is 1 if subchain  $i$  is allowed to execute on core  $j$ . Given the exponential solution space, we add a constraint for tractability: each subchain either runs alone on one or more cores or shares a single core with other subchains (i.e. two or more subchains do not share two or more cores). We also add a trivial constraint: each subchain should be assigned to at least one core, and vice versa.

We begin with estimating the period  $p_i$  of the subchain  $S_i$ , as a function of  $a_{ij}$  variables. The period of a subchain captures its execution rate; subchain  $S_i$  processes a new input every  $p_i$  time units. We consider two cases (based on the above constraints), and make simplifying assumptions in each case for computational tractability — we relax these assumptions when making finer-grained scheduling decisions in Stage II (§5.2).

<sup>8</sup>We allow the constraints to be soft, i.e. if the scheduler cannot meet them, it prints a warning, and aims to meet a looser (scaled up) set of constraints.

Chain $C_t: S_{t1} \rightarrow S_{t2}..S_{tn}$ , with periods $p_{t1}..p_{tn}$	
Metric	Approximation
Chain Latency	$p_{t1} + \sum_{x=2}^n 2 * p_{tx}$
Chain Throughput	$1 / (\max_{x=1}^n p_{tx})$
Chain Response Time	Latency + $1 / \text{Throughput}$

**Table 1.** Approximate formulae for chain-level metrics. Note that we use the worst case latency formula, and average throughput (the exact time gap between two outputs can vary in practice). These simple approximations allow us to formulate the problem as MILP and GP in Stages I and II respectively.

(i) If multiple subchains share a single core  $x$ , we assume each subchain gets an equal share of the CPU core (inspired by Linux’ fair scheduling [17, 18]). The period of a subchain  $S_i$  that is assigned to core  $x$  will then be the sum of computation time of all nodes in  $S_i$  multiplied by the number of subchains that are sharing the core  $x$ .

(ii) If a subchain  $S_i$  is assigned  $k_i$  cores ( $k_i \geq 1$ ), we assume all nodes in  $S_i$  have the same degree of parallelism (i.e. all nodes can be parallelized to use  $q$  cores, where  $1 \leq q \leq k_i$ ) and their compute scales perfectly with it. We use the analytical formulation described later in §5.2 to compute the period  $p_i$  based on the computation time of each node in the subchain.

Thus, for a given core allocation  $a_{ij}$ , we get approximate periods  $p_i$  for each subchain  $S_i$ . We next estimate the chain-level and node-level metrics as a function of  $p_i$  for each subchain which, in turn, allows us to estimate the final objective function as a function of  $a_{ij}$ . For a subchain  $S_i$  with period  $p_i$ , the throughput of each node in  $S_i$  is equal to the subchain’s throughput, i.e.  $1/p_i$ . Table 1 lists how we estimate chain-level metrics, for a chain  $C_t$  comprising of subchains  $S_{t1} \rightarrow S_{t2} \rightarrow S_{t3}..S_{tn}$ . The average chain throughput is bottlenecked by its slowest subchain. We estimate the worst-case chain latency as follows: at each subchain  $S_{ti}$  in the chain, a new output  $o_{t(i-1)}$  from the preceding subchain ( $S_{t(i-1)}$ ) might have to wait for a whole period, (i.e.  $p_{ti}$ ) for  $S_{ti}$  to finish its current execution (except for at  $S_{t1}$  where there’s no waiting time), and it will take  $p_{ti}$  time for  $S_{ti}$  to fully process  $o_{t(i-1)}$  and produce a new output.<sup>9</sup> We then estimate the chain response time as the sum of the chain latency and period (reciprocal of throughput).

Using the models above, we formulate a Mixed Integer Linear Program (MILP) that solves for  $a_{ij}$  such that the specified objective function is optimized. Intuitively, the solver determines the right trade off of which subchains can share a single core vs which ones should be allowed to scale up to multiple cores, based on the specified weights and constraints.

## 5.2 Stage II: Per Core and Per Subchain Scheduling

Given the subchain to core mappings from our first optimization stage, the next stage makes finer-grained scheduling decisions for each subchain and core. We consider two cases:

<sup>9</sup>It is a common practice in real-time literature [60] to compute worst case latency of chains in this manner.

**Single subchain on one or more cores.** For a subchain  $S_i$  comprising of nodes  $\{n_{i1}, n_{i2}, ..n_{im}\}$  with  $k_i$  assigned cores, the scheduler computes the time period  $p_i$  of the source node ( $n_{i1}$ ) and the degree of parallelism for a node in the subchain ( $q_i$ ), such that the response time along the subchain is minimized.

The period of the subchain corresponding to a given value of  $q \in [1, k_i]$  is given by:

$$p_i(q) = \max(\max_{j=1}^m (c_{ij}^q), \sum_{j=1}^m (c_{ij}^q) / \lfloor k_i / q \rfloor) \quad (1)$$

where  $c_{ij}^q$  is  $n_{ij}$ ’s computation time with at most  $q$  cores (only a subset may be designed to use all  $q$ ). Note that, unlike period computation in Stage 1, we allow different nodes in the subchain to use different degrees of parallelism in this stage.

The corresponding response time of the subchain, for a given  $q$ , can be analytically computed as  $(\sum_{j=1}^m (c_{ij}^q) + p_i(q))$ . We iterate over all possible values of  $q \in [1, k_i]$  and select the value  $q_i$  (and the corresponding  $p_i$ ) that results in lowest response time for the subchain. We have proved that this rate allocation achieves subchain response time within  $2 \times$  the optimal, and equal to the optimal if all the nodes in the subchain can only use a single thread (i.e.  $q_i = 1$ ) [2].

**Multiple subchains on a single core.** For subchains  $S_1, S_2..S_n$  assigned the same core, the scheduler must determine their periods and temporal allocation of CPU time across them. We construct a periodic schedule, and execute  $f_i$  fraction of subchain  $S_i$  in each period, such that  $\sum_{i=1}^n (f_i * c(S_i))$  equals the period of the schedule, where  $c(S_i)$  is the sum of computation time for all nodes in  $S_i$ . The execution of each (fractional) subchain within a period follows a configurable ordering.<sup>10</sup> Each subchain will finish processing one input once every  $1/f_i$  periods, i.e.  $p_i = \frac{\sum_{i=1}^n (f_i c(s_i))}{f_i}$ . We allow  $f_i$  to be larger than 1 for subchains that require optimizing *average* throughput (e.g. GL in robot navigation)<sup>11</sup>, and constrain  $1/f_i$  to be an integer for other subchains to allow the scheduler to control the exact throughputs. We combine the above period formula with metric estimations given in Table 1, and formulate a Geometric Programming problem to compute the  $f_i$  and  $p_i$  variables such that the specified objective function is optimized under the specified constraints.

## 5.3 Handling Variations

**Coarse Grained Variations.** We handle coarse-grained variations over time by continually recording the computation time across all nodes and tracking the number of available cores. We re-compute the stage II scheduling decisions (§5.2) periodically using the 95%ile computation time for each node measured over the previous 50 values in our implementation. We handle multimodal computation times by

<sup>10</sup>By default, Catan assigns the order based on specified weights, but provides an option to directly specify it as a semantic input.

<sup>11</sup>We cannot assume a fixed time period of input processing for nodes that buffer and batch process inputs, and instead consider their average throughput. Such nodes can either be auto-identified (given support from framework) or can be explicitly identified by the developer.

taking the weighted sum of 95%ile computation times across the different modes. We invoke the more expensive stage I optimization (§5.1) less frequently.

**Fine Grained Variability.** In spite of periodically adapting the scheduling decisions, a node may still exceed its expected (previously measured) computation time. To handle these situations, the scheduler implements a priority-based stealing mechanism, wherein if nodes  $A$  and  $B$  share a core, and  $B$  has lower priority than  $A$ , then in each period of the schedule, the scheduler allocates  $B$ 's CPU time to  $A$  if the last output from  $A$  was not received at its expected time period. We infer node priorities from the specified weights, and also provide the option to explicitly specify these as semantic inputs.

## 6 Implementation

We implement Catan scheduler on top of Linux, as a ROS node for robotics and as an ILLIXR plugin for VR, both of which use the same backend which handles all the scheduling decisions.

**Initialization.** At initialization time, Catan requires the DAG structure and the thread ids corresponding to each node, since they are required to enforce fine grained scheduling. Note that both of the above inputs can be automatically obtained by adding hooks to the framework. For robotics, we modify the ROS communication library [31] to expose the ids of all the threads it uses under-the-hood to handle communication between nodes.

**Bootstrapping.** Catan takes the application DAG and constraints/weights as input, and bootstraps the core allocation by assigning equal compute time to all the nodes and running the Stage - I solver.<sup>12</sup> Based on the output, Catan spawns a thread  $TQ_j$  for each core with multiple subchains, and a thread  $TS_i$  for every subchain assigned to one or more cores, to handle the per-core and per-subchain scheduling respectively. It bootstraps the per core fractional schedule by assigning a fraction of 1 to all subchains. The bootstrapped configuration lasts only for the first 2s, until actual node computation times are measured and the solver is invoked. Lastly, it spawns a dynamic re-optimization thread which periodically updates the scheduling decisions. All the scheduler threads ( $TQ_j$  and  $TS_i$ ) are assigned the SCHED\_FIFO policy with a very high priority of 4, except for the re-optimization thread which runs with the SCHED\_OTHER policy, so as not to interfere with the application's execution.

**Runtime.** At runtime, each scheduler thread  $TS_i$  triggers the first (source) node of the subchain  $i$  at the analytically computed time period. The threads  $TQ_j$  enforce the core  $j$ 's periodic fractional schedule using two mechanisms. First, it triggers the first node in each subchain  $s_y$  once every period if  $f_y \geq 1$ , and once every  $1/f_y$  periods otherwise. Secondly, in each period of the schedule, it assigns SCHED\_FIFO policy with the lowest priority of 1 to all the node threads, and

<sup>12</sup>We set same compute times of all nodes at bootstrap, so as to share the CPU equally among all nodes (the exact value, set to 5ms, does not matter).

iteratively bumps up the SCHED\_FIFO priority (to 2) of (all the threads of) each subchain for the computed fraction of its time within the period. As described in §5.3, the controller can enforce priority-based stealing within each period. For threads that we do not schedule explicitly, (e.g. IMU in ILLIXR which needs to run at high frequency and has negligible compute), we assign SCHED\_FIFO policy with a fixed high priority (3) so that they can preempt any node whenever needed<sup>13</sup>.

The scheduler takes 0.12ms to pause the execution of one node, and start executing the next. We add an extra constraint on each subchain  $c(s_i) * f_i \geq 1$  to limit the scheduler's intervention (and the ensuing overhead due to that). We also add 5% slack time in each period, which can be used by the re-optimization thread or the application threads.<sup>14</sup> We scale the analytical functions for the low level metrics accordingly, in both the optimization formulations.

**Dynamic Re-optimization.** We periodically re-solve for the new optimal scheduling decisions, based on the latest compute time estimates of all nodes (as discussed in 5.3). We have implemented both the MILP and GP formulations using the Mosek Fusion C++ library. It takes our solver 24-26ms to solve the GP for the navigation application and 5-6ms for VR. Solving the MILP is more expensive, requiring 60ms for the navigation DAG for 2 cores. We invoke both the solvers 2s after initialization, and then re-run Stage I every 20s, and Stage II every 5s. Increasing the time periods can decrease the overhead of running the solvers. We chose the periods so as to keep the overhead roughly under 0.05 CPU cores<sup>15</sup>. For each execution of the Stage I optimization, if the core allocation changes, then we kill the existing  $TQ_j$  and  $TS_i$  threads and re-initialize them based on the new solution. We kill the threads for simplicity, and observe negligible overheads due to this, but the implementation can be updated to send information to the existing threads instead of killing them.

## 7 Evaluation

### 7.1 Face Tracking

Our first study highlights the importance of scheduling decisions in sense-react systems in the absence of complex semantic trade-offs and variability.

**Scheduler Configuration.** As the app comprises of only a single chain, the scheduling objective is to minimize its response time. All app nodes belong to the same subchain.

**Experiment Setup.** We use Gazebo [9] (a standard physics simulator used for evaluating robotics applications) to simulate a dummy moving along a square path centered at a robotic camera that can rotate at a velocity of up to 3.2rad/s

<sup>13</sup>One could use Linux' SCHED\_DEADLINE scheduler to implement Catan's scheduling decisions instead of SCHED\_FIFO, but we found it to be too inflexible for handling variations.

<sup>14</sup>This is done to account for the fact that Linux does not allow SCHED\_FIFO processes to use more than 95% CPU time [18].

<sup>15</sup>The process of selecting the solver periods can easily be automated based on this criteria by tracking the solvers' compute usage.



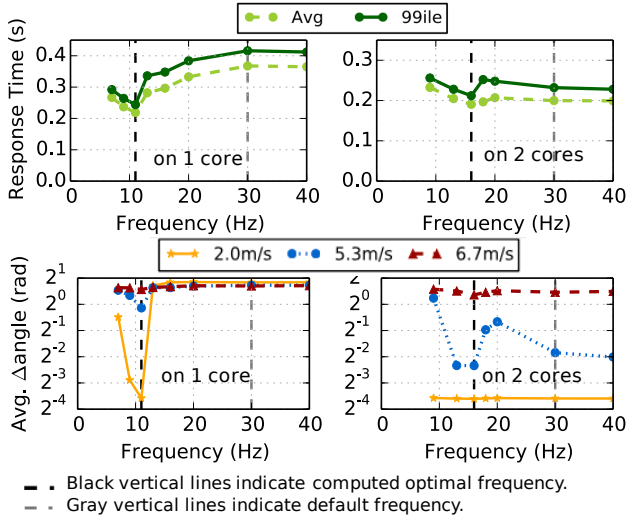


**Figure 6.** Response time (top) and tracking performance for different object speeds (bottom) as source frequency is varied.

([42, 43]). Gazebo feeds camera inputs to detection and planning nodes implemented in ROS, which in turn feed the velocity output back to the simulated camera.

We run the whole setup (i.e. the simulator as well as the application) on an AWS EC2 instance (m5.4xlarge). Gazebo runs on 5 reserved cores, and sends camera inputs as fast as it can to a shim source node, which models the time taken for post-processing or formatting camera inputs (measured as 25ms using the usb-cam module [34]) and then publishes the latest input at the specified frequency. Since the algorithm to detect the simulated dummy is trivial, we model realistic timings by augmenting our detection node – every time it processes a simulated frame, it also runs a single-cascade HAAR algorithm [32, 78] on a frame drawn from a real video data-set [59, 87] (the time taken for this varies between 55-60ms). The planning node (which takes 1ms) tracks the dummy using the detection output from the simulated frame. We experiment with varying source frequency and speed at which the dummy moves, as well as with different number of cores  $k$  made available to the application (that excludes Gazebo).

**Baselines.** We compare Catan to the default configuration, which is based on the source frequency hand-tuned by the application developer (30 Hz) and uses Linux’ default policy SCHED\_OTHER (based on Completely Fair Scheduler) for all other scheduling decisions. This configuration remains the same regardless of the number of cores.

**Metrics.** We evaluate Catan on the chain response time as well as the robot’s face tracking performance. We measure the tracking performance as average angular distance ( $\Delta$ angle) between the camera’s orientation and the position of the dummy (a lower value implies better performance).

**Results.** Figure 6 shows the response time and tracking performance for a range of source frequencies on a system with one and two cores (to model platforms with limited

compute). The black and gray vertical lines indicate the optimal value assigned by Catan, and the default configuration respectively. The compute capacity is the bottleneck with one core, while the slowest node is the bottleneck with two cores.

Response time (shown in the top graphs) is lowest at the optimal source frequency computed by Catan using the analytical formulation in §5.2. This is because a lower than optimal frequency lowers throughput of the chain, while higher than optimal frequency increases latency (detailed explanation omitted for brevity).

We draw the following key observations with respect to the tracking performance (shown in the bottom graphs): (i) Tracking performance strongly correlates with the response time, confirming the impact of low-level metrics on app performance. (ii) The system has the best tracking performance when running at the optimal frequency configured by Catan, outperforming the default configuration. This shows the impact of scheduling on app performance. (iii) In general, it is harder to track a faster moving object. Catan’s optimal frequency is able to track the object for wider speed ranges.

## 7.2 Robot Navigation

**Scheduler Configuration.** We model the objective function as the weighted sum of response times for the different chains involving each node in the navigation DAG (detailed below), and the average output period for GL (i.e. the average time interval at which it processes scans) as a measure of its throughput. We do not explicitly schedule odometry, and configure Scan  $\rightarrow$  LM  $\rightarrow$  LP as a single subchain. All other nodes shown in Figure 2 (i.e. GL, GM, GP, and NC) are treated as individual subchains, that can run at different rates. The analytical response times for the local chains (involving the LM and LP) sourced at scans and at odometry differ only by a constant (odometry’s period) – we combine them into a single response time metric for our objective function, assigning it the highest weight of 1.0 (as they are responsible for avoiding collisions). We use a weight of 0.5 for GL’s average output period (to ensure freshness of pose estimates and odometry for path planning). In addition to these, our objective function includes the response time along three chains that include the three remaining processing nodes (GM, GP, NC) sourced at GL – each assigned a small weight of 0.005 (to ensure that these nodes are not starved as the local chain and GL are prioritized).<sup>16</sup> We also add the following application specific constraints into our optimization formulation: (i) GL’s average throughput must be at most 50Hz, based on the maximum frequency at which the simulator can publish laser scans. (ii) GP’s throughput must be at most 1Hz.

**Experiment Setup.** We use Stage [37] to simulate a P3AT robot [26]. The simulator feeds laser scans and odometry into the navigation application, which is implemented on top of ROS [33]. The application feeds the robot’s velocity

<sup>16</sup>When analytically computing response times along the chains sourced at GL, the scheduler uses the empirically observed value of the rate at which it outputs filtered scans (1.5Hz at 75%ile).

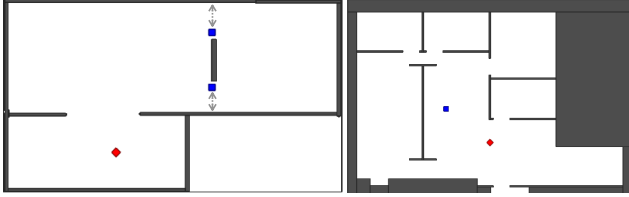


**Figure 7.** Map 1 (left) and Map 2 (right) used for navigation experiments. The blue squares represent the obstacles and the red square represents the robot. The obstacles in Map1 are dynamic, and move along the two doorways.

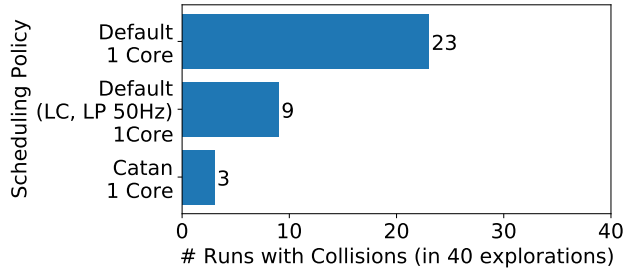


**Figure 8.** No. of runs with collisions (out of 40) on Map1, with (i) Default config, (ii) Default with LC, LP at 50Hz, and (iii) with Catan,

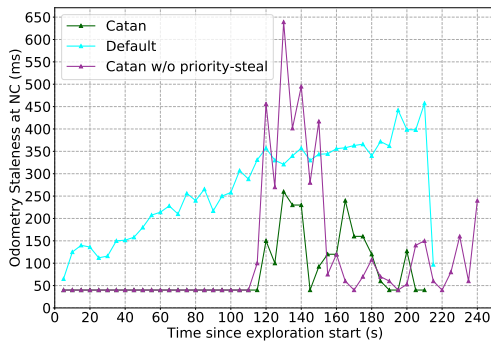


**Figure 9.** Tail odometry staleness at NC on Map2 for Catan vs Default vs Catan w/o priority stealing (median over 20 runs).

back into Stage. We configure the simulator to publish laser scans and odometry at 50Hz. We conduct experiments on two maps: (i) Map 1 (Figure 7(left)) requires the robot to move around a dynamic obstacle at the entrances of a room (this models realistic scenarios where collisions with dynamic obstacles may occur at narrow doorways). This map allows us to evaluate the ability of the robot to avoid collisions with dynamic obstacles under different configurations. (ii) Map 2 (Figure 7(right)) requires the robot to explore a larger area. We do not add any dynamic obstacles to this map, focusing on other performance metrics. Unless otherwise specified, all nodes run on a system with one core (it is common for robots to have single / dual core on-device compute [26]).

#### Comparison with manually-tuned configuration.

**Baselines.** We begin with comparing the performance of Catan with the default configuration (manually-tuned by the developer of the navigation app). In line with the interface

currently exposed by ROS, the default configuration only specifies the execution rate of each node [33] (set to 5Hz for LM, 10Hz for LP, 0.2Hz for GM, upto 1Hz for GP, 10Hz for NC), relying on Linux’ default policies (SCHED\_OTHER based on Completely Fair Scheduler) for other scheduling decisions. **Metrics.** We evaluate Catan against the default configuration on the robot’s performance for both Map1 and Map2. For Map1, we do 40 experiment runs and compare the number of runs in which the robot collides with an obstacle. For Map2, we compare the staleness of odometry used for generating navigation command and the area exploration rate. We capture odometry staleness by recording the time difference between an odometry reading and when the corresponding pose is used by NC. For each experiment run, we aggregate the staleness values collected over time buckets of 5s by computing the 95%ile values. For each 5s bucket, we report the median of these values across 20 runs. We define the area exploration rate as the time taken to explore 90% of the map area, averaged over 20 runs. We omit the comparison of low-level metrics for brevity, but Catan is able to achieve better response time for all chains.

**Map1 Results.** Figure 8 compares the number of experiment runs (out of a total of 40) in which the robot collides with an obstacle on Map1. With the default configuration (which runs the LM and LP at low rates of 5 Hz and 10 Hz), more than 50% runs suffer from collisions. Increasing the rate of LM and LP nodes to 50 Hz reduces the number of collision to 9. With a high weight assigned to the response time along the local chain, Catan is able to run the local chains at an even higher rate (125 - 170 Hz), reducing the number of collisions to only 3. These results highlight the impact of scheduling decisions on a robot’s performance.

**Map2 Results.** Figure 9 shows the odometry staleness metric. We find that, in general, Catan has lower odometry staleness than the default policy. When GL’s compute usage spikes up (especially during loop closures) and as the compute load increases over time (due to increased CPU usage for GM and GP), Catan is able to explicitly prioritize GL over GM and GP due to its periodic adaptation and priority-based stealing. We isolate the impact of priority-based stealing by disabling it for GL (results shown with the pink line in Figure 9). Disabling priority-based stealing increases staleness, as the the scheduler cannot handle sudden spikes in GL due to loop closure.

The above results show how Catan performs better than the default configuration with respect to avoiding collisions and ensuring freshness of odometry readings. Improvements in these more critical metrics come at the cost of a small reduction in the area exploration rate – the time taken to explore 90% of the area increases by 10.9%, as GM is allocated smaller amount of resources in Catan than in the default scheme. Thus, Catan achieves the desired trade-offs, as per the configured weights and priorities.

#### Adapting to variations in resource usage over time.

We next highlight the importance of updating scheduling decisions over time, as resource usage changes. We extend the

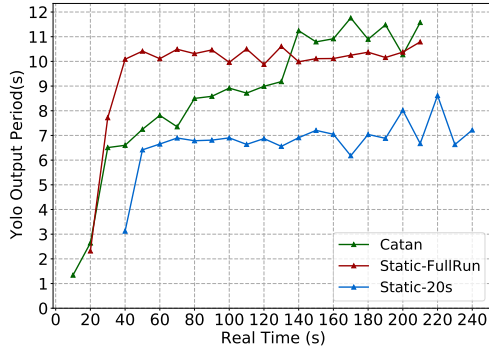


**Figure 10.** The output period (as a measure of reciprocal of throughput) for the YOLO chain across three schemes: Catan, and two static baselines Static-FullRun and Static-20s on 1 core. We report the median of average period over 20 runs.

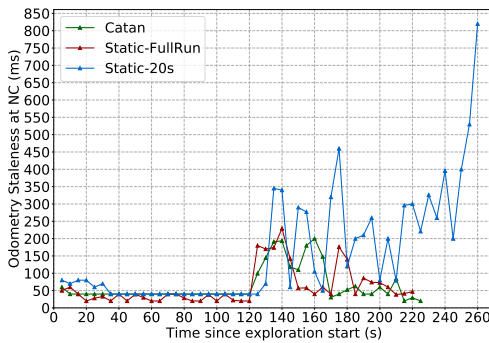


**Figure 11.** Comparing tail odometry staleness at NC (median over 20 runs) on Map2 across three schemes: Catan, and two static baselines Static-FullRun and Static-20s on 1 core.

navigation DAG by adding another chain that runs an object detector on camera images as the robot moves around (this is representative of robotic tasks, such as ObjectGoal task [50]). The chain comprises of a pre-processing node (similar to the one used in §7.1) and a YOLO object detection node [80]<sup>17</sup>. To model realistic timings in the simulated environment, we feed images from a real image dataset [61] to the object detection node. We augment our objective function for Catan to include the response time along this chain as another metric with a very low weight of 0.0005. We run this extended navigation application on a system with one core.

**Baselines.** We compare Catan with two baselines that use a static configuration (that is not updated over time): (i) Static-FullRun that uses the same optimization problem as Catan based on the tail computation time for each node over an entire experiment run on Map2 using a single core. It computes the schedule once, and does not re-solve it periodically. Note that since computation times of GM and GP nodes increase as the run progresses, this scheme uses a schedule derived from over-estimated computation time towards the beginning of the run. (ii) Static-20s is similar to Static-Full, but uses tail computation times of each node over the first 20s of

<sup>17</sup>While YOLO is usually GPU based, we don't run it on GPU since we focus on CPU scheduling. We leave CPU/GPU co-scheduling [89] to future work.

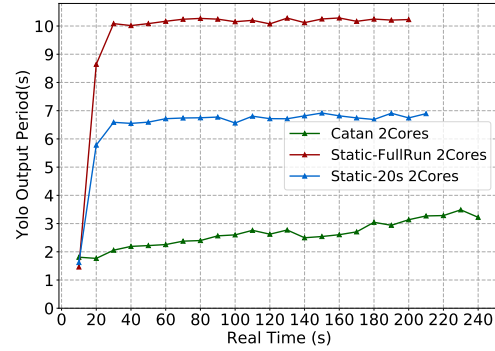


**Figure 12.** The output period (as a measure of reciprocal of throughput) for the YOLO chain across three schemes: Catan, and two static baselines static-FullRun and Static-20s on 2 cores.

the run. This scheme would use a schedule derived from an under-estimated computation time in the later half of the run. **Metrics.** We desire the objects to be detected in real time at a high rate, but that should not come at the cost of not being able to navigate well. Hence, we evaluate Catan and the baselines on multiple metrics – number of collisions in 40 runs on Map1 and, odometry staleness at NC, area exploration rate and the average output period for the YOLO chain (as a measure of reciprocal of its throughput) over 20 runs on Map2. To aggregate YOLO chain's throughput data across 20 runs, we first take the average period (measured as the time gap between two consecutive outputs from the YOLO chain) over 10s buckets for each run, and then plot the median of these average values for each bucket.

**Results.** Figure 10 shows the average output period for the YOLO chain over runs on Map2 – lower is better. We find that Static-FullRun, which overestimates the computation time of navigation nodes in the first half of the run, assigns a low rate to the YOLO chain (resulting in high output period in the first half). Static-20s, which underestimates the computation of navigation nodes (by looking at the values in the first 20s of a run), assigns a high rate to YOLO – as we discuss next, this comes at the cost of worse performance on a more critical metric. Catan, with its dynamic re-solving assigns a high rate (low period) to YOLO at the beginning of the run, and then gradually decreases the rate (increases the period) over time.

Figure 11 shows the odometry staleness at navigation command across the three schemes run on Map2. While Static-FullRun and Catan both perform similarly on this metric, Static-20s exhibits higher staleness towards the second half of the run. By using under-estimated computation times for the second half, Static-20s mis-allocates resources, giving a smaller share of CPU time to GL, GM, and GP, and a more than necessary amount of CPU resources to the local chain nodes, NC, and YOLO. This reduces the effective throughput of GL (in spite of priority-based stealing) and increases odometry staleness.

All three schemes performed similarly with respect to avoiding collisions on Map1, and in terms of the area exploration rate, and so we omit detailed results.

**Adapting to change in resource availability.** Our experiments so far used a single core. We next ran the extended navigation application (with the YOLO chain) on Map2 on a system with two cores, to evaluate how well Catan auto-scales. *Baselines.* We configured the system to use the same node execution rates as those computed by the two baselines above (i.e. Static-FullRun and Static-20s with static schedules derived from node computation times on Map2 on one core), relying on default Linux policies to schedule the nodes across two cores. *Metrics.* We compare the average output period for the YOLO chain over time, as defined previously.

*Results.* Figure 12 plots the average output period for the YOLO chain over time across Catan and the two baselines on 2 cores. We find that Catan is able to make efficient use of the extra core – it dynamically allocates the core to just the local chain in the first half, and the local chain and GP in the second half. It is, thus, able to run YOLO at a higher rate (and lower output period) than other static baselines that do not increase the execution rates.

**Key Takeaways.** (i) Scheduling decisions impact how well a robot can navigate an environment while avoiding collisions. (ii) Catan achieves the desired trade-offs across different metrics. (iii) It is important to adapt scheduling decisions over time and as resource availability changes – Catan is able to do so by dynamically re-solving the schedule over time. (iv) It is important to adapt to sudden fine-grained variability in resource usage – Catan is able to do so via priority based stealing.

### 7.3 Virtual Reality

**Scheduler Configuration.** We model the objective function as a weighted sum of response times for various chains in the VR DAG. We model IMU  $\rightarrow$  Int as a subchain but do not explicitly schedule it since it has negligible compute time and executes at a high frequency. We configure Camera  $\rightarrow$  VIO as a single subchain (since only VIO uses Camera’s output). The remaining nodes, Timewarp and Render are individual subchains. We use a weight of 1 and 0.5 for the chains IMU  $\rightarrow$  Int  $\rightarrow$  Timewarp and IMU  $\rightarrow$  Int  $\rightarrow$  Render  $\rightarrow$  Timewarp respectively (these chains are more important, corresponding to rotational and translational motion-to-photon response time respectively). For all the remaining (4) chains that go through VIO, we use a weight of 0.005. We also add throughput constraints as per the display refresh rate (vsync, determined by the display hardware and driver): (i) Timewarp’s rate is upper and lower-bounded by vsync. (ii) Render’s rate is upper-bounded by vsync. The order of the subchains is specified to be Timewarp followed by Camera  $\rightarrow$  VIO, then Render, so that each render output is as close to the next timewarp execution as possible. We enable priority-based stealing only for timewarp, i.e. it is not preempted and can steal CPU time from the other nodes if needed.

**Experiment Setup.** We use the ILLIXR system for our VR application [13, 66]. As discussed in § 3.3, we use a standard dataset for the camera and IMU inputs to ILLIXR for repeatability. We use Vicon Room 1 Medium from

EuRoC [56], which consists of an 85 second long trajectory, and provides camera images at 20 Hz and IMU readings at 200 Hz. The Render component renders a custom scene consisting of a living room with furniture and textured walls. We use a display with a resolution of 2560x1440, and a refresh rate of 120 Hz (vsync period of 8.33 ms). We run the CPU parts of our setup on a single core of an Intel i9-10900K CPU clocked at 5.3 GHz. The GPU parts execute on an NVIDIA GeForce RTX 3090 with a core clock of 2.1 GHz.

**Baselines.** We compare Catan against two baselines. The first baseline configures static rates (Timewarp and Render running at vsync frequency and Camera running at the frequency of the image dataset) and relies on Linux default policy SCHED\_OTHER for all other scheduling decisions. The second baseline extends the first one, by using SCHED\_FIFO for all the nodes and prioritizing the execution of different components in the following order: IMU and Int (so that they run at the dataset’s high frequency), followed by TW, then Render and then Camera and VIO (based on decreasing order of their chains’ weights).

**Metrics.** We compare the response time along the chains (A) IMU  $\rightarrow$  Int  $\rightarrow$  Timewarp (that captures rotational MTP), (B) IMU  $\rightarrow$  Int  $\rightarrow$  Render  $\rightarrow$  Timewarp (that captures translational MTP), and (C) Camera  $\rightarrow$  VIO  $\rightarrow$  Int  $\rightarrow$  Timewarp (that captures how quickly accurate pose-information is available from VIO). For each scheme, we first average the metrics within each run over time, and then depict the average and standard deviation of these values across 20 runs.

**Results.** Figure 13 compares the two baselines with Catan. We make the following observations: (i) The priority stealing mechanism in Catan enables it to execute Timewarp just before vsync in spite of variations in computation times of different nodes, leading to better response time by  $\approx 7\%$ . (ii) Catan’s temporal CPU allocation to Render ensures that it finishes execution as close to vsync as possible, leading to  $\approx 25\%$  improvement in chain B response time. (iii) Lastly, our system is able to trigger Camera at a high rate,<sup>18</sup> while continually adapting to varying compute times, without affecting the rest of the system due to its explicitly planned schedule, leading to  $\approx 11\%$  improvement in chain C. Overall, Catan is able to make the desired trade-offs across different components in the application.

## 8 Related Work

System scheduling has a rich literature. We discuss three broad (and most closely related) categories, highlighting their limitations in addressing the requirements for sense-react systems. *Real-time scheduling.* Prior work in real-time scheduling for DAGs assumes static periodic schedules, and focus on meeting latency constraints under given (and fixed) time periods at which a node is triggered [53, 83, 98, 99] (including

<sup>18</sup>Even though the offline dataset has a fixed camera input rate, sending triggers for camera at a higher rate reduces delay due to asynchrony between offline camera inputs and triggers. We expect to see similar (and potentially larger) benefits with live camera inputs.

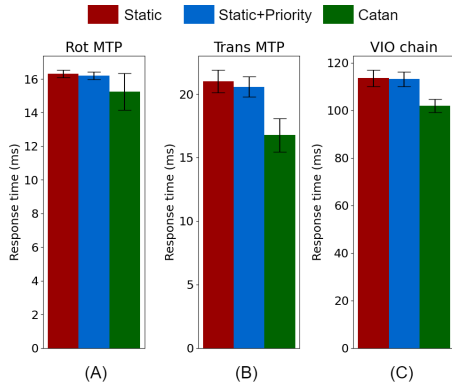


**Figure 13.** Response time of the chains processing (A) approx. rotational motion, (B) approx. translational motion, and (C) accurate motion via VIO. The error bars show one standard deviation above and below. These results are aggregated over 20 runs.

the few that look at robotics applications [58, 84, 93, 100]. Davare et al. [60] focus on assigning per-node time periods in automotive applications but under given node priorities and core allocations. These works use expensive algorithms, and do not account for variability in processing times.

*Stream-processing systems.* Many stream processing engines make scheduling decisions locally at each node (which are often suboptimal) [28, 46, 47, 72, 73, 95, 96]. Among those that make system-wide decisions, most focus on resource allocation or task scheduling to handle a given (though variable) input load (e.g. [57, 67, 77, 85]). A few look at input load shedding to avoid system overload, but do not simultaneously optimize resource allocation and task ordering (e.g. [52, 91]). More generally, such mechanisms are designed for a different application domain and environment (e.g. query processing in cloud clusters), and do not optimize for the application-level goals in resource-constrained sense-react systems.

*Sensor Nodes.* Pixie [74] is an operating system for sensor nodes, which provides a dataflow programming model with abstractions for managing resources - but leaves all the scheduling decisions upto the application. Flask [75] also uses a dataflow model to define a Domain Specific Language for sensor network applications, but does not handle variations in compute usage or availability. While Eon [88] provides a flexible interface to express how the scheduling parameters can be adapted at runtime, it requires the developer to specify how to change each parameter based on different resource availability. More generally, none of the sensor node systems deal with complex compute or fine grained variability.

*Offline profiling.* Some of the data-driven approaches rely on extensive offline profiling to tune different aspects of the system configuration (e.g. [51, 55, 64, 68, 101]). However, such approaches cannot adapt to dynamic variations over time and across deployment scenarios. Nonetheless, extending such data-driven approaches to handle the requirements of sense-react systems is an interesting future direction.

## 9 Conclusion

In this work, we build an understanding of the scheduling requirements and challenges for sense-react systems by studying three applications spanning robotics and VR. Using this understanding, we develop a scheduler to manage on-device CPU resources for sense-react applications. We show how it is able to handle multiple scheduling dimensions across heterogeneous app nodes, adapt to variations in compute resource usage at different timescales, and achieve the specified semantic trade-offs.

We believe our work to be a first step in a rich problem domain of sense-react system scheduling, with multiple interesting questions open for future research. For instance, Catan currently requires several inputs from the app developers, e.g. performance constraints and objectives along different components of an application. While we believe that specifying such high-level inputs is still significantly easier than configuring low-level system knobs (as required today), an important direction for future research includes automatically inferring these inputs (e.g. via data-driven approaches) to further ease app development.

As mentioned in §2, extending our scheduler (currently restricted to managing CPU resources on a single platform) to handle other resources (e.g. GPU, accelerators, etc), varying deployment models (e.g. tasks offloaded to edge or cloud servers) as well as different frameworks (e.g. ROS 2) is another interesting future direction.

## Acknowledgements

This work was supported by Intel, AG NIFA under grant 2021-67021-34418, the Applications Driving Architectures (ADA) Center, a JUMP Center co-sponsored by SRC and DARPA, the DARPA DSSOC program, and NSF under grants 2120464 and 2008971.

## References

- [1] Qualcomm Snapdragon XR2 5G Platform. <https://www.qualcomm.com/products/snapdragon-xr2-5g-platform>.
- [2] Anonymized link for supplementary proofs. <https://drive.google.com/file/d/1mnblovU2UMb9fdQzEQszPRWPBUHv9CH/view?usp=sharing>.
- [3] AWS Robomaker. <https://aws.amazon.com/robomaker/>.
- [4] Clearpath Robotics. <https://clearpathrobotics.com/>.
- [5] CORBA. <https://www.corba.org/>.
- [6] da Vinci Si Surgical Robot. <https://med.nyu.edu/robotic-surgery/physicians/what-robotic-surgery>.
- [7] Fetch Robotics. <http://docs.fetchrobotics.com/FetchRobotics.pdf>.
- [8] Fetch Robotics Specification. <http://docs.fetchrobotics.com/FetchRobotics.pdf>.
- [9] Gazebo. <http://gazebo.org/>.
- [10] Hansen Medical. <https://www.aurishealth.com/hansen-medical>.
- [11] How Drones Are Being Used to Battle Wildfires. <https://www.smithsonianmag.com/videos/category/smithsonian-channel/drones-are-now-being-used-to-battle-wildfires/>.
- [12] Htc vive pro. <https://www.vive.com/us/product/vive-pro/>.
- [13] ILLIXR (Illinois Extended Reality testbed) Consortium. <https://illixr.org>.

- [14] Introduction to mobile robotics - slam. <http://ais.informatik.uni-freiburg.de/teaching/ss12/robotics/slides/12-slam.pdf>.
- [15] LCM. <https://lcm-proj.github.io/>.
- [16] Lessons learned building a self-driving car on ROS, Cruise Automation. [https://roscon.ros.org/2018/presentations/ROSCon2018\\_LessonsLearnedSelfDriving.pdf](https://roscon.ros.org/2018/presentations/ROSCon2018_LessonsLearnedSelfDriving.pdf).
- [17] Linux Completely Fair Scheduler. <https://www.kernel.org/doc/html/latest/scheduler/sched-design-CFS.html>.
- [18] Linux CPU Scheduling - Limiting the CPU usage of real-time and deadline processes. <https://man7.org/linux/man-pages/man7/sched.7.html>.
- [19] LoCoBot. <http://www.locobot.org/>.
- [20] NVIDIA Isaac SDK. <https://developer.nvidia.com/isaac-sdk>.
- [21] NVIDIA Jetson: Embedded Systems for Next-Generation Autonomous Machines. <https://www.nvidia.com/en-in/autonomous-machines/embedded-systems/>.
- [22] Oculus Go. <https://www.oculus.com/go/>.
- [23] Oculus Quest 2. <https://www.oculus.com/quest-2/>.
- [24] Openxr. <https://www.khronos.org/openxr/>.
- [25] OROCOS. <http://www.orocos.org/>.
- [26] P3AT Robot. <https://www.generationrobots.com/media/Pioneer3AT-P3AT-RevA-datasheet.pdf>.
- [27] Qualcomm Snapdragon 835 Mobile Platform. <https://www.qualcomm.com/products/snapdragon-835-mobile-platform>.
- [28] RabbitMQ. <https://www.rabbitmq.com/>.
- [29] Rapyuta Robotics. <https://www.rapyuta-robotics.com/>.
- [30] ROS. <https://www.ros.org/>.
- [31] ROS Communication Library. [http://wiki.ros.org/ros\\_comm](http://wiki.ros.org/ros_comm).
- [32] ROS Face Tracking. [http://wiki.ros.org/face\\_detection\\_tracking](http://wiki.ros.org/face_detection_tracking).
- [33] ROS Navigation2D Application (Source: [https://github.com/skasperski/navigation\\_2d](https://github.com/skasperski/navigation_2d)). <http://wiki.ros.org/nav2d>.
- [34] ROS Usb cam : Driver for USB cameras. [http://wiki.ros.org/usb\\_cam](http://wiki.ros.org/usb_cam).
- [35] ROSA Knee System. <https://www.zimmerbiomet.com/medical-professionals/knee/product/rosa-knee.html>.
- [36] ROS:Community Metrics Report. <http://download.ros.org/downloads/metrics/metrics-report-2018-07.pdf>.
- [37] Stage Simulator. <http://playerstage.sourceforge.net/doc/Stage-3.2.1/>.
- [38] Terrasentia : The automated crop monitoring robot. <https://blog.plantwise.org/2018/07/17/terrasentia-the-automated-crop-monitoring-robot/>.
- [39] Tesla Autopilot. <https://www.tesla.com/autopilot>.
- [40] TurtleBot. <https://www.turtlebot.com/>.
- [41] TurtleBot 3 . <https://emanual.robotis.com/docs/en/platform/turtlebot3/features/#specifications>.
- [42] Turtlebot3 Robot Actuators. <https://emanual.robotis.com/docs/en/platform/turtlebot3/specifications/#actuators>.
- [43] Turtlebot3 Robot Actuators Specifications. <https://emanual.robotis.com/docs/en/dxl/x/xm430-w210/>.
- [44] Turtlebot3 Waffle Pi. <https://www.robotis.us/turtlebot-3-waffle-pi/>.
- [45] Waymo. <https://waymo.com/>.
- [46] ZeroMQ. <http://zeromq.org/>.
- [47] Daniel J. Abadi, Yanif Ahmad, Magdalena Balazinska, Ugur Cetintemel, Mitch Cherniack, Jeong-Hyon Hwang, Wolfgang Lindner, Anurag S. Maskey, Alexander Rasin, Esther Ryvkina, Nesime Tatbul, Ying Xing, and Stan Zdonik. The Design of the Borealis Stream Processing Engine. In *CIDR 2005*.
- [48] R. Aggarwal, T. P. Grantcharov, J. R. Eriksen, D. Bliurup, V. B. Kristiansen, P. Funch-Jensen, and A. Darzi. An evidence-based virtual reality training program for novice laparoscopic surgeons. *Ann Surg*, 244(2):310–314, Aug 2006.
- [49] Amazon Robotics. <https://www.amazonrobotics.com/#/>.
- [50] Peter Anderson, Angel Chang, Devendra Singh Chaplot, Alexey Dosovitskiy, Saurabh Gupta, Vladlen Koltun, Jana Kosecka, Jitendra Malik, Roozbeh Mottaghi, Manolis Savva, et al. On evaluation of embodied navigation agents. *arXiv preprint arXiv:1807.06757*, 2018.
- [51] J. Ansel, S. Kamil, K. Veeramachaneni, J. Ragan-Kelley, J. Bosboom, U. O’Reilly, and S. Amarasinghe. Opentuner: An extensible framework for program autotuning. In *2014 23rd International Conference on Parallel Architecture and Compilation Techniques (PACT)*, pages 303–315, 2014.
- [52] Brian Babcock, Mayur Datar, and Rajeev Motwani. Load shedding for aggregation queries over data streams. In *ICDE ’04: Proceedings of the 20th International Conference on Data Engineering*, 2004.
- [53] S. Baruah, V. Bonifaci, A. Marchetti-Spaccamela, L. Stougie, and A. Wiese. A generalized parallel task model for recurrent real-time processes. In *2012 IEEE 33rd Real-Time Systems Symposium*, pages 63–72, 2012.
- [54] Raunak P. Bhattacharyya, Derek J. Phillips, Changliu Liu, Jayesh K. Gupta, Katherine Driggs-Campbell, and Mykel J. Kochenderfer. Simulating emergent properties of human driving behavior using multi-agent reward augmented imitation learning. In *2019 International Conference on Robotics and Automation (ICRA)*, pages 789–795, 2019.
- [55] Muhammad Bilal and Marco Canini. Towards automatic parameter tuning of stream processing systems. In *Proceedings of the 2017 Symposium on Cloud Computing, SoCC ’17*, page 189–200, New York, NY, USA, 2017. Association for Computing Machinery.
- [56] Michael Burri, Janosch Nikolich, Pascal Gohl, Thomas Schneider, Joern Rehder, Sammy Omari, Markus W Achtelik, and Roland Siegwart. The EuRoC micro aerial vehicle datasets. *The International Journal of Robotics Research*, 35(10):1157–1163, 2016.
- [57] Don Carney, Uğur Çetintemel, Alex Rasin, Stan Zdonik, Mitch Cherniack, and Mike Stonebraker. Operator scheduling in a data stream manager. In *Proceedings of the 29th International Conference on Very Large Data Bases - Volume 29, VLDB ’03*, page 838–849. VLDB Endowment, 2003.
- [58] Hyun-Seon Choi, Yecheng Xiang, and Hyoseung Kim. Picas: New design of priority-driven chain-aware scheduling for ros2. *2021 IEEE 27th Real-Time and Embedded Technology and Applications Symposium (RTAS)*, pages 251–263, 2021.
- [59] G. G. Chrysos, E. Antonakos, S. Zafeiriou, and P. Snape. Offline deformable face tracking in arbitrary videos. In *2015 IEEE International Conference on Computer Vision Workshop (ICCVW)*, pages 954–962, 2015.
- [60] Abhijit Davare, Qi Zhu, Marco Di Natale, Claudio Pinello, Sri Kanajan, and Alberto Sangiovanni-Vincentelli. Period optimization for hard real-time distributed automotive systems. In *Proceedings of the 44th annual Design Automation Conference*, pages 278–283, 2007.
- [61] Mark Everingham, Luc Gool, Christopher K. Williams, John Winn, and Andrew Zisserman. The pascal visual object classes (voc) challenge. *Int. J. Comput. Vision*, 88(2):303–338, June 2010.
- [62] P. Fitzpatrick, E. Ceseracciu, D. Domenichelli, A. Paikan, G. Metta, and L. Natale. A middle way for robotics middleware, 2014.
- [63] Patrick Goebel. *ROS By Example*. Lulu, 2013.
- [64] Herodotos Herodotou, Fei Dong, and Shivnath Babu. No one (cluster) size fits all: Automatic cluster sizing for data-intensive analytics. In *Proceedings of the 2nd ACM Symposium on Cloud Computing, SOCC ’11*, New York, NY, USA, 2011. Association for Computing Machinery.
- [65] Guoqiang Hu, Wee Peng Tay, and Yonggang Wen. Cloud robotics: architecture, challenges and applications. *IEEE network*, 2012.
- [66] Muhammad Huzaifa, Rishi Desai, Samuel Grayson, Xutao Jiang, Ying Jing, Jae Lee, Fang Lu, Yihan Pang, Joseph Ravichandran, Finn Sinclair, Boyuan Tian, Hengzhi Yuan, Jeffrey Zhang, and Sarita V. Adve. Exploring extended reality with ILLIXR: A new playground for architecture research. In *2021 IEEE International Symposium on Workload Characterization (To Appear)*. A prior version of this work appears in CoRR abs/2004.04643, March 2021.

- [67] Michael Isard, Mihai Budiu, Yuan Yu, Andrew Birrell, and Dennis Fetterly. Dryad: Distributed data-parallel programs from sequential building blocks. In *Proceedings of the 2nd ACM SIGOPS/EuroSys European Conference on Computer Systems 2007*, EuroSys '07, page 59–72, New York, NY, USA, 2007. Association for Computing Machinery.
- [68] P. Jamshidi and G. Casale. An uncertainty-aware approach to optimal configuration of stream processing systems. In *2016 IEEE 24th International Symposium on Modeling, Analysis and Simulation of Computer and Telecommunication Systems (MASCOTS)*, pages 39–48, 2016.
- [69] Ben Kehoe, Sachin Patil, Pieter Abbeel, and Ken Goldberg. A survey of research on cloud robotics and automation. *IEEE Transactions on automation science and engineering*, 2015.
- [70] KiwiBot. <https://www.kiwicampus.com/>.
- [71] Stephan Krohn, Johanne Tromp, Eva M Quinque, Julia Belger, Felix Klotzsche, Sophia Rekers, Paul Chojecki, Jeroen de Mooij, Mert Akbal, Cade McCall, Arno Villringer, Michael Gaebler, Carsten Finke, and Angelika Thöne-Otto. Multidimensional evaluation of virtual reality paradigms in clinical neuropsychology: Application of the vr-check framework. *J Med Internet Res*, 22(4):e16724, Apr 2020.
- [72] Sanjeev Kulkarni, Nikunj Bhagat, Maosong Fu, Vikas Kedigehalli, Christopher Kellogg, Sailesh Mittal, Jignesh M Patel, Karthik Ramasamy, and Siddarth Taneja. Twitter heron: Stream processing at scale. In *Proceedings of the 2015 ACM SIGMOD International Conference on Management of Data*, pages 239–250, 2015.
- [73] Wei Lin, Zhengping Qian, Junwei Xu, Sen Yang, Jingren Zhou, and Lidong Zhou. Streamscope: Continuous reliable distributed processing of big data streams. In *13th USENIX Symposium on Networked Systems Design and Implementation (NSDI 16)*. USENIX Association, 2016.
- [74] Konrad Lorincz, Bor-rong Chen, Jason Waterman, Geoff Werner-Allen, and Matt Welsh. Resource aware programming in the pixie os. In *Proceedings of the 6th ACM Conference on Embedded Network Sensor Systems*, SenSys '08, page 211–224, New York, NY, USA, 2008. Association for Computing Machinery.
- [75] Geoffrey Mainland, Greg Morrisett, and Matt Welsh. Flask: Staged functional programming for sensor networks. In *Proceedings of the 13th ACM SIGPLAN International Conference on Functional Programming*, ICFP '08, page 335–346, New York, NY, USA, 2008. Association for Computing Machinery.
- [76] Morgan McGuire. “exclusive: How nvidia research is reinventing the display pipeline for the future of vr, part 1. 2017.
- [77] Derek G. Murray, Frank McSherry, Rebecca Isaacs, Michael Isard, Paul Barham, and Martín Abadi. Naiad: A timely dataflow system. In *Proceedings of the Twenty-Fourth ACM Symposium on Operating Systems Principles*, SOSP '13, page 439–455, New York, NY, USA, 2013. Association for Computing Machinery.
- [78] Michael Jones Paul Viola. Rapid object detection using a boosted cascade of simple features. In *Proceedings of the 2001 IEEE computer society conference on computer vision and pattern recognition. CVPR 2001*, 2001.
- [79] Morgan Quigley, Ken Conley, Brian P Gerkey, Josh Faust, Tully Foote, Jeremy Leibs, Rob Wheeler, and Andrew Y Ng. Ros: an open-source robot operating system. 2009.
- [80] Joseph Redmon, Santosh Divvala, Ross Girshick, and Ali Farhadi. You only look once: Unified, real-time object detection. In *Proceedings of the IEEE Conference on Computer Vision and Pattern Recognition (CVPR)*, June 2016.
- [81] Roomba. <https://www.irobot.com/roomba>.
- [82] Stuart Russell and Peter Norvig. *Artificial intelligence: a modern approach 4th edition*. 2020. <http://aima.cs.berkeley.edu/index.html>.
- [83] A. Saifullah, K. Agrawal, C. Lu, and C. Gill. Multi-core real-time scheduling for generalized parallel task models. In *2011 IEEE 32nd Real-Time Systems Symposium*, pages 217–226, 2011.
- [84] Y. Saito, F. Sato, T. Azumi, S. Kato, and N. Nishio. Rosch: real-time scheduling framework for ros. In *2018 IEEE 24th International Conference on Embedded and Real-Time Computing Systems and Applications (RTCSA)*, pages 52–58, 2018.
- [85] M. J. Sax, M. Castellanos, Q. Chen, and M. Hsu. Performance optimization for distributed intra-node-parallel streaming systems. In *2013 IEEE 29th International Conference on Data Engineering Workshops (ICDEW)*, pages 62–69, 2013.
- [86] Wolfram Burgard Sebastian Thrun and Dieter Fox. *Probabilistic Robotics*. MIT Press, 2005. <https://mitpress.mit.edu/books/probabilistic-robotics>.
- [87] J. Shen, S. Zafeiriou, G. G. Chrysois, J. Kossaifi, G. Tzimiropoulos, and M. Pantic. The first facial landmark tracking in-the-wild challenge: Benchmark and results. In *2015 IEEE International Conference on Computer Vision Workshop (ICCVW)*, pages 1003–1011, 2015.
- [88] Jacob Sorber, Alexander Kostadinov, Matthew Garber, Matthew Brennan, Mark D. Corner, and Emery D. Berger. Eon: A language and runtime system for perpetual systems. In *Proceedings of the 5th International Conference on Embedded Networked Sensor Systems*, SenSys '07, page 161–174, New York, NY, USA, 2007. Association for Computing Machinery.
- [89] Yuhei Suzuki, Takuya Azumi, Shinpei Kato, and Nobuhiko Nishio. Real-time ros extension on transparent cpu/gpu coordination mechanism. *2018 IEEE 21st International Symposium on Real-Time Distributed Computing (ISORC)*, pages 184–192, 2018.
- [90] Ajay Kumar Tanwani, Nitesh Mor, John Kubiawicz, Joseph E. Gonzalez, and Ken Goldberg. A fog robotics approach to deep robot learning: Application to object recognition and grasp planning in surface decluttering. *CoRR*, abs/1903.09589, 2019.
- [91] Nesime Tatbul, Uğur Çetintemel, Stan Zdonik, Mitch Cherniack, and Michael Stonebraker. Load shedding in a data stream manager. In *Proceedings of the 29th International Conference on Very Large Data Bases - Volume 29, VLDB '03*, page 309–320. VLDB Endowment, 2003.
- [92] J.M.P. van Waveren. The asynchronous time warp for virtual reality on consumer hardware. In *Proceedings of the 22nd ACM Conference on Virtual Reality Software and Technology*, pages 37–46. ACM, 2016.
- [93] Micaela Verucchi, Mirco Theile, Marco Caccamo, and Marko Bertogna. Latency-aware generation of single-rate dags from multi-rate task sets. In *2020 IEEE Real-Time and Embedded Technology and Applications Symposium (RTAS)*, pages 226–238. IEEE, 2020.
- [94] Daniel Wagner. Motion to Photon Latency in Mobile AR and VR, 2018.
- [95] Matt Welsh and David Culler. Adaptive overload control for busy internet servers. In *Proceedings of the 4th conference on USENIX Symposium on Internet Technologies and Systems*, 2003.
- [96] Matt Welsh, David Culler, and Eric Brewer. Seda: An architecture for well-conditioned, scalable internet services. In *Proceedings of the Eighteenth ACM Symposium on Operating Systems Principles*, SOSP '01, page 230–243, New York, NY, USA, 2001. Association for Computing Machinery.
- [97] Brian Yamauchi. A frontier-based approach for autonomous exploration. In *Proceedings 1997 IEEE International Symposium on Computational Intelligence in Robotics and Automation CIRA'97. Towards New Computational Principles for Robotics and Automation*, pages 146–151. IEEE, 1997.
- [98] M. Yang, T. Amert, K. Yang, N. Otterness, J. H. Anderson, F. D. Smith, and S. Wang. Making openvx really "real time". In *2018 IEEE Real-Time Systems Symposium (RTSS)*, pages 80–93, 2018.
- [99] Y. Yang, A. Pinto, A. Sangiovanni-Vincentelli, and Q. Zhu. A design flow for building automation and control systems. In *2010 31st IEEE Real-Time Systems Symposium*, pages 105–116, 2010.
- [100] Yuqing Yang and Takuya Azumi. Exploring real-time executor on ros 2. In *2020 IEEE International Conference on Embedded Software and Systems (ICCESS)*, pages 1–8, 2020.
- [101] Haoyu Zhang, Ganesh Ananthanarayanan, Peter Bodik, Matthai Philipose, Paramvir Bahl, and Michael J. Freedman. Live video analytics at scale with approximation and delay-tolerance. In *14th USENIX*

, , Aditi Partap, Samuel Grayson, Muhammad Huzaifa, Sarita Adve, Brighten Godfrey, Saurabh Gupta, Kris Hauser, and Radhika Mittal

*Symposium on Networked Systems Design and Implementation (NSDI*

*17)*. USENIX Association, 2017.